EFFECT OF FRICTION-STIR PROCESSING ON THE WEAR BEHAVIOR OF TITANIUM (Ti-1Al-8V-5Fe) AND STAINLESS STEEL (A-286) ALLOYS

Olusegun Olukunle Tinubu, B.Sc.

Thesis Prepared for the Degree of

MASTER OF SCIENCE

UNIVERSITY OF NORTH TEXAS

May 2015

APPROVED:

Thomas W. Scharf, Major Professor
Rajiv Mishra, Committee Member
Samir M. Aouadi, Committee Member
Andrey Voevodin, Chair of the Department of Material Science and Engineering
Costas Tsatsoulis, Dean of the College Engineering and Interim Dean of the Toulouse Graduate School

Tinubu, Olusegun Olukunle. *Effect of Friction-Stir Processing on the Wear Behavior of Titanium (Ti-1Al-8V-5Fe) and Stainless Steel (A-286) Alloys*. Master of Science (Materials Science and Engineering), May 2015, 39 pp., 20 figures, 6 tables, 22 numbered references.

The effect of friction stir processing (FSP) on the mechanical wear behavior was investigated for Ti-1Al-8V-5Fe (Ti-185) and stainless steel (Incoloy® A-286) alloys. The Ti-185 and A-286 alloys were tested in different processing conditions, including as rolled (AR), AR+FSP, and AR+FSP+aged. A high frequency reciprocating rig was used to simulate fretting-type wear of these alloys at room temperature. The Vickers micro-hardness and wear rates were calculated and compared for each processing condition. It was determined that along with increasing hardness in the stir zones, FSP resulted in improved wear resistance for both alloys. Specifically, wear rates in the stir zones were reduced to lowest values of 1.6×10^{-5} and 5.8×10^{-7} $mm^3/N \cdot m$ for the AR+FSP+aged Ti-185 and A-286 alloys, respectively, despite lower hardness for A-286 alloy. Mechanistic studies were conducted to determine the reason behind these improvements in wear resistance and the effect of FSP on the microstructural evolution during wear. For the Ti-185 alloy, x-ray diffraction revealed that there was a phase transformation from β-Ti (AR+FSP) to α-Ti (AR+FSP+aged). This β-phase decomposition resulted in the harder and stiffer α-Ti phase responsible for lowering of wear rate in Ti-185. While x-ray diffraction confirmed the A-286 alloy retains its austenitic structure for all conditions, scanning electron microscopy revealed completely different wear track morphology structures. There was increased coarse abrasion (galling) with the AR+aged A-286 alloy compared to the much finer-scale abrasion with the AR+FSP+aged alloy, which was responsible for smaller and less abrasive wear debris, and hence lower wear rate. Furthermore, cross-sectional focused ion beam microscopy studies inside the stir zone of AR+FSP+aged A-286 alloy determined that a)

increased micro-hardness was due to FSP-induced microscopic grain refinement, and b) the corresponding wear rate decrease was due to even finer wear-induced grain refinement. With both effects combined, the level of damage and surface fatigue wear was suppressed resulting in lowering of the wear rate. In contrast, the absence of FSP-induced grain refinement in the AR+aged A-286 alloy resulted in lower hardness and increasing wear rate. In addition, micro-Raman spectroscopy inside the stir wear zone determined that the wear debris contained metal oxides of Fe_3O_4, Cr_2O_3, and NiO, but were a consequence and not the cause of low wear. Overall, FSP of titanium and stainless steel alloys resulted in lowering of wear rates suggesting it is a viable surface engineering technique to target and mitigate site-specific wear.

ACKNOWLEDGEMENTS

I give glory to the almighty God for seeing me through this work.

To my supervisor professor Dr. Thomas Scharf whom I can't even thank enough for everything he did for me throughout the course of my program. He took me in and was very patient with me and gave me a lot of chances as I got better and better. To Dr Samir Aouadi and Dr Rajiv Mishra, thank you for taking time out of your busy schedule to serve on my thesis committee and I appreciate your contributions. To Shami, Aniket, and Ved, thank you for helping with the FSP and Hardness testing.

To my parents, thank you for the financial help, encouragements and also for believing in me, only our almighty God can repay you. To my sisters, Omowumi and Damola, thank you for all the sacrifices, encouragements and prayers.

I would like to appreciate Dr. Victor Ageh for being there for me as a brother, helper, and an encourager from the first day I set my foot into the university, you inspired me in a lot of ways and I thank God I met you. To my lab mates and friends Jon and Nneoma, for their steady encouragement and help with part of my work, I say thank you. I would also love to acknowledge the wonderful friends I made here at UNT, Charles, Aditya, Av, Femi, Riad, Bharat, Aku, Jonova, Jithendra, Andres, Seun, Gbemi, Ryan, Dayo, Adaku and others, I love you all.

TABLE OF CONTENTS

LIST OF TABLES

LIST OF FIGURES

CHAPTER 1

INTRODUCTION AND LITERATURE REVIEW

Tribology is a multi-disciplinary scientific and engineering field based on the interaction of two or more surfaces in relative motion, such as in sliding and rolling contacts. Many material phenomena, such as strain hardening, phase transformations, and tribochemical reactions, occur at the interface in both dry and lubricated contacts. These events affect the materials wear, friction and lubrication behavior. When these interactions happen, the changed surfaces can result in increased friction and wear. The importance of tribology is to understand and find solutions to the challenges encountered during these interactions. Through microstructural modification at and near the surface, friction stir processing (FSP) can be used to increase the surface hardness of alloys and hence may improve the sliding wear resistance [1,2].

Friction stir processing (FSP) is a process that was developed based on the foundation of friction stir welding (FSW) [1,2]. It is a relatively new solid-state processing technique that improves the surface hardness of metallic alloys through surface microstructural modification, such as strain hardening and grain refinement. This process is a variant of the friction stir welding (FSW) process used for solid joining of two separate or different pieces of metallic materials. It involves the use of a non-consumable rotating tool with a pin and shoulder inserted into a single piece of material and allowed to travel along the desired path to cover the area of interest. The result of this process enhances or changes the microstructure of the desired area that is typically a result of plastic deformation, and also the exposure of heat to the alloy that may lead to recrystallization. The qualities and characteristics of FSP have allowed its use for microstructural modification in several metallic alloys. The near surface properties improvement by the use of

friction stir processing (FSP) is expected to have several effects on the tribological behavior of the processed surface of the materials [3,4].

FSP has been applied to many different alloys, including Al, Mg, Cu, Fe, and Ni-based alloys with their results showing improvements in their mechanical and tribological properties [3-10]. Maloney and Lynch [11] used FSP to enhance the mechanical properties of various alloys determining that (a) the strength of cast nickel-aluminum-bronze was doubled, (b) there was a five times increase in ductility of alloy A356, and (c) fatigue life increased for the fusion welds. In general, the benefit of increasing mechanical hardness of metals and alloys in improving the wear resistance has its roots in Archard's wear equation [12]:

$$\boldsymbol{V} = \left(\frac{\boldsymbol{k}}{\boldsymbol{H}}\right)\boldsymbol{Ld} \qquad (1)$$

where V is material wear volume loss, k is the wear coefficient, H is the hardness of the softer metal, L is the normal load and d is the total sliding distance. Equation 1 was initially established for adhesive wear involving shearing or breaking of adhesive junctions between contacting surfaces, but also applies to abrasive wear involving scratching by asperities or entrapped debris. In both modes, V is proportional to L and d and inversely proportional to H, i.e. the harder the metal, the lower the wear volume loss. Therefore, it is conjectured that increased hardness due to FSP may result in improved wear resistance.

To understand the wear behavior of any sliding alloy, there are many factors and conditions that need to be considered, including the set conditions of the experiment, how they interact with their environment and also properties of the alloys. A lot of work has been performed on the characterization of sliding wear mechanism of metallic alloys including aluminum and titanium alloys. Titanium alloys, such as Ti–6Al–4V, are mostly used in the aerospace and biomedical

industries because of high biocompatibility, very good strength, good corrosion resistance and also low density [13,14]. A very essential application of Ti–6Al–4V is its use for bone and other medical implants in the human body. There has been focus on this material to enhance its strength without reducing the ductility [15,16]. Knowing that the wear performance of any alloy depends strongly on the surface layer, the aim to modify the surface of these alloys by increasing mechanical strength and hardness could result in improved wear resistance of these alloys [7,17]. FSP is a method that has been identified as a solution and has already attracted considerable attention in multiple industries due to its unique process advantages and high success for joining processing of many alloys [18]. Budinski [19] studied the wear behavior of Ti-6Al-4V under fretting conditions against different counterfaces, such as self-mated, cemented carbide, stainless steel and chromium plate. The damage to the counterface was assessed by profilometry, and wear scar depths were measured for all members and volume loss was calculated from the data. The results suggested that this alloy was subjected to more damage when it was used in self-mated contacts and also against stainless steels [19]. However, this study did not implement surface engineering techniques, such as FSP, to change the near surface microstructure to improve tribo-mechanical properties.

In addition, components that are produced by aluminum and its alloys exhibit poor tribological behavior. Hence, there have been attempts to develop new Al-based materials with better resistance to wear. In these cases, FSP has been identified to achieve this by also surface hardening due to grain refinement [17]. In addition, Song et al [18] investigated the microstructure and mechanical properties of a surface modified Inconel 718, a Ni-Cr alloy, using FSP and determined that surface grain refinement improved its yield and tensile strength. Other methods have been used in increasing the hardness of various steels, such as nitriding, heat treatment and

carburizing. However, these methods do not acknowledge the material loss in steels [8] and they are very energy and often capital intensive [3]. Other drawbacks with these techniques are the entire sample must be treated, as opposed to the surface only, and thermal distortion can occur resulting in distortion of the sample. FSP circumvents these issues since it is a surface engineering process used to improve hardness, toughness, fatigue resistance and wear resistance of various steels, such as 52100 steel, 4140 steel, and AISI 420 martensitic stainless steel [3,4,8,10]. Lorenzo-Martin et al [3] performed experiments to study the use of FSP to harden the surface of AISI 4140 steel and also compare the results with the above mentioned conventional thermal treatments. They determined that FSP of steel showed a tribological improvement compared to conventional thermal treatment, in which the FSP treated surfaces wore two times less than conventional heat treated surfaces. This improvement in wear resistance and surface hardening was attributed to grain refinement, phase transformation from austenite to hardened martensite, and increased carbon solubility [3]. The increase in surface hardness in the stirred region reduced the extent of abrasion and the grain refinement, which is expected to mitigate surface fatigue wear when compared to surface hardening by the above mentioned thermal treatments.

In this thesis, FSP was applied to titanium (Ti-1Al-8V-5Fe) and iron-nickel-chromium (Incoloy® A-286) alloys to determine if similar improvements in the mechanical and tribological properties occurred and what fundamental mechanisms are responsible for such improvements. Such studies on these alloys have not been performed to date. A high frequency reciprocating rig (HFRR) was used to simulate the fretting wear behavior of these alloys. Fretting wear occurs when two contact surfaces that are usually at rest are subjected to short amplitude reciprocating sliding, which can accelerate crack nucleation of working components to lead to premature catastrophic failures [20]. Since vibration is one of the main causes of the fretting movement, it follows that

the most likely areas for it to occur is in machinery such as contacts between hubs, shrink- and press-fits, and bearing housings on loaded rotating shafts or axles [21,22].

The aim of this study is to present the results of experiments on the fretting-type wear behavior of alloys Ti-1Al-8V-5Fe and A-286 stainless steel at room temperature and the effect FSP has on the microstructural evolution during wear. The Ti-1Al-8V-5Fe was tested in different forms, including the as rolled, as rolled+FSP, as rolled+FSP+aged conditions. The A-286 alloy was also examined in different forms, including as rolled+aged and as rolled+FSP+aged. The hardness and wear rates/factors for each condition were calculated and compared and electron microscopy and vibrational spectroscopy were used to determine how FSP affects microstructural and chemical evolution during wear, respectively, that are responsible for these mechanical and tribological properties.

CHAPTER 2

MATERIALS AND EXPERIMENTAL PROCEDURES

2.1 Materials and Preparation

2.1.1 Ti-1Al-8V-5Fe (Ti-185) Alloy

Rolled Ti-185 plates acquired from RTI International were used as base material. The as-received sheet had a thickness of ~5.05 mm. Figure 2.1 shows a schematic of the friction stir welding (FSW) tool that was used for friction stir processing (FSP) of the alloys.

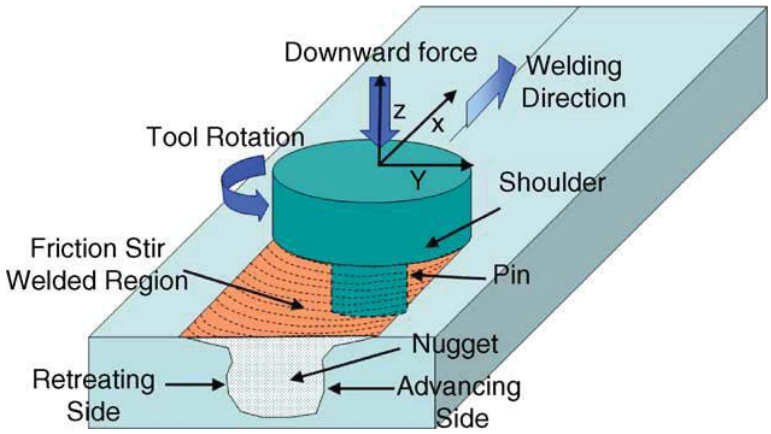

Figure 2.1. Schematic of FSW machine for FSP of alloys [R.S. Mishra et al, Department of Materials Science and Engineering, University of North Texas,].

The FSP experimental conditions are summarized in Table 2.1.

Tool used	Rotational speed (RPM)	Traverse speed (RPM)
W-La_2O_3	600	2

Table 2.1: FSP conditions for Ti-185 alloy.

FSP was performed by using a smooth W–1%La_2O_3 tool with shoulder diameter, pin diameter and pin length of 10.1 mm, 6.1 mm, and 1.7 mm, respectively. A 2.51 tilt opposite the traveling direction was applied to the pin tool for all the processing. During processing, argon gas shielding was applied for the prevention of Ti–185 samples from oxidation. The first sample was in as rolled condition (*as rolled*), and the second was in as rolled condition and was further processed using the FSP machine (*as rolled+FSP*). This latter sample was also aged by heating to 300°C for 2 hrs and was allowed to cool to ambient by normal air cooling. It was then heated again to 500°C for 8 hrs followed by cooling to ambient (*as rolled+FSP+aged*). All three of these treated alloys were ~4 mm thick.

2.1.2 A-286 Alloy

Incoloy® A-286 is an iron-based austenitic, precipitation hardened alloy primarily composed of iron-nickel-chromium with additions of molybdenum and titanium. Table 2.2 lists the chemical composition of the A-286 alloy. The alloy is known in general for its high strength and oxidation/corrosion resistance at temperatures up to ~700°C, thereby making it useful for various components of aircraft, e.g. gas turbines, and automotive, e.g. engine and manifold fastener applications.

Nickel.....24.0-27.0
Iron .....Balance*
Chromium.....13.5-16.0
Titanium.....1.90-2.35
Molybdenum.....1.0-1.5
Vanadium.....0.10-0.50
Carbon .....0.08 max.
Manganese .....2.0 max.

Silicon .....1.0 max.

Aluminum.....0.35 max.

Sulfur.....0.030 max.

Boron.....0.001-0.01

Table 2.2: Chemical composition of A-286 (wt %).

Rolled A-286 plates were acquired from California Technologies. The as received sheet had a thickness of ~3.2 mm. The FSP runs were conducted with a polycrystalline cubic boron nitride (PCBN) tool. The PCBN tool had a pin length of 5 mm, a pin diameter of 7.6 mm, and a shoulder diameter of 23.8 mm. The FSP conditions are summarized in Table 2.3.

Tool used	Rotational speed (RPM)	Traverse speed (RPM)
PCBN	400	1

Table 2.3: FSP conditions for A-286 alloy.

Furthermore, the alloy was treated in a solution at 900°C for 2 hrs and was allowed to cool to ambient. This was followed by age hardening through heating at 720°C for about 16 hrs and cooling to ambient (*as rolled+FSP+aged*). The second treated alloy was in as rolled condition and was aged by heating the sample to 300°C for 2 hrs and allowed to cool to ambient; followed by heating again to 720°C for about 16 hrs and cooled to ambient (*as rolled+aged*).

2.2 Characterization

2.2.1 X-ray Diffraction (XRD)

XRD was used to identify the phases and crystal structure in Ti-185 and A-286 alloys for all processing conditions. A Rigaku Ultima III diffractometer was used in both normal and grazing/glancing angle incidence mode. For glancing angle mode, the settings in the parallel beam mode used a thin film stage and a scintillation detector. CuKα x-rays with a wavelength of 0.154 nm were generated at 40 kV and 44 mA. Scans were carried out between 20 to 90° 2θ, 5° incident angle, 0.05° step size, 2 degree/min scan speed, 10 mm divergence height limiting slit, 0.5° incident side Soller slit, open attenuator, 0.5° diffracted side parallel beam (PB) slit, and 1 mm sizes for all divergence, scattering and receiving slits (DS/SS/RS). For normal mode, scans were done between 20 to 90° 2θ, omega and settings were kept at 5^0 incident angle, 0.05 step size, 2 degree/minute scan speed, 5° incident side soller sit, 5° receiving soller slit, 5-mm divergence height slit, all attenuators were opened. The data collected was then processed using Jade v9.0 software and compared to known powder diffraction files (PDF) for the phases.

2.2.2 Micro Hardness Testing

Micro hardness measurements were performed on Ti-185 and A-286 using a Shimadzu Vickers hardness tester. The tests were performed at room temperature. Measurements were taken at three different distances from the top edge at 2.0, 4.0 and 4.5 mm after post weld aging and FSP. Normal loads of 500 and 100 grams were used for Ti-185 and A-286, respectively, at an acquisition time of 10 seconds.

2.2.3 Wear Testing

A high frequency reciprocating rig (HFRR) from PCS Instruments, shown in Figure 2.2, was used to simulate the fretting-type wear behavior of the alloys. Figure 2.3 shows a high

magnification image of the test setup with contacting surfaces. A silicon nitride (Si_3N_4) ball counterface (diameter of 6.35 mm) was used in all experiments. The HFRR conditions were set at a normal load at 0.2 N (equivalent to an average Hertzian contact pressure of 0.35 GPa), stroke length of 1 mm, reciprocating frequency of 20 Hz, and total sliding distance was 216 m. All experiments were carried out at room temperature of 25^{o}C and humidity (~50% RH) for 90 mins per test. For repeatability purposes, at least five HFRR measurements were taken for each alloy. The Si_3N_4 balls were cleaned with acetone and distilled water prior to each test. Pictures of the ball surface and the wear tracks were acquired with an Olympus U-TV0 optical microscope.

Figure 2.2. Image of HFRR experimental set up to simulate fretting-type wear [Source: PCS Instruments]

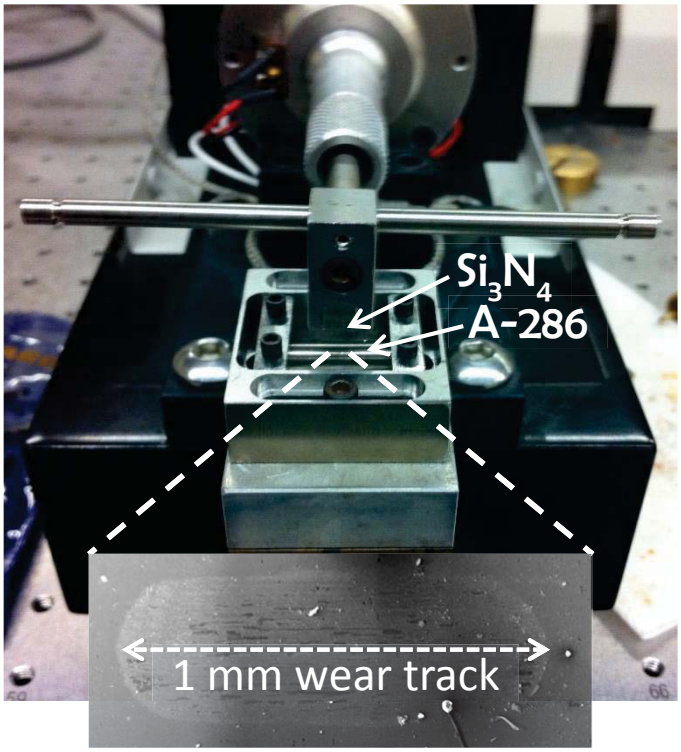

Figure 2.3. Image of HFRR set up showing Si_3N_4 ball in contact with A-286 alloy. Inset shows representative 1 mm long stroke length of the wear track.

2.2.4 Profilometry

After wear testing, a Veeco Dektak 150 Profilometer was used to measure the wear track depths and cross-sectional areas of each alloy. The stylus pin of the profilometer has a ~12.3 μm radius, and a force of 100 μg was applied during the scans. The cross-sectional worn area data was used to calculate the wear factor/rate of the tracks. At least five profilometry traces were taken inside each wear track to obtain cross-sectional wear areas. The wear factor (WF), in units of $mm^3/N \cdot m$, is calculated as

$$Wear Factor (WF) = \frac{volume loss}{load \bullet distance} \equiv \left(\frac{mm^3}{N \bullet m} \right)$$

2.2.5 Scanning Electron Microscopy and Focused Ion Beam Machining

An FEI-Nova 200 dual beam Scanning Electron Microscope/Focused Ion Beam (SEM/FIB) system was used to image the surfaces of the A-286 and Ti-185 alloys. Images of the cross-sections inside and outside the wear tracks were also taken after HFRR testing to determine the microstructural evolution during wear inside the FSP nugget regions shown in Figure 2.1. The ion beam was operated at 5 kV with an emission current of 1.6 nA. Electron e-beam Pt followed by ion i-beam Pt were deposited on the alloy surfaces prior to FIB milling to protect the surfaces from Ga ion implantation.

CHAPTER 3

RESULTS AND DISCUSSION

3.1 X-Ray Diffraction (XRD)

Figure 3.1 shows an XRD scan of the Ti-185 alloy before and after friction stir processing (FSP), and also after FSP with precipitation hardening (Aging). The peaks of the as-rolled (AR) sample show the existence of a mixture of α-Ti (HCP) and β-Ti (BCC) phases. The β-Ti phase is more predominant based on the x-ray intensities. After the AR sample is friction stirred, XRD shows evidence of FSP-induced texturing with (110) β-Ti preferred orientation. With a subsequent aging step, there was further microstructural evolution in the AR+FSP+aged alloy with β-phase decomposition, shown in Figure 3.1. This phase transformation resulted in the presence of the harder and stiffer α-Ti phase, which will be shown in the following sections to be responsible for lowering of the wear rate in this processed Ti-185 alloy.

Figure 3.2 shows the XRD scan of the stainless steel A-286 alloy. The scan shows that despite friction stir processing and aging, there was no change in the microstructure for the AR+aged and AR+FSP+aged samples. FCC austenite (γ) is the only phase present. This phase was indexed with the powder diffraction file (PDF) number 03-065-5131, a solid solution phase containing Fe and Ni in the ratio of Fe_3Ni_2 ($F\,m\bar{3}m$ space group 225). This Fe_3Ni_2 stoichiometry is similar to the Fe and Ni fractional content in the A-286 alloy. Unlike the Ti-185 alloy that exhibited a phase transformation during FSP and aging, XRD confirmed that the A-286 alloy retained its austenitic structure during both FSP and aging.

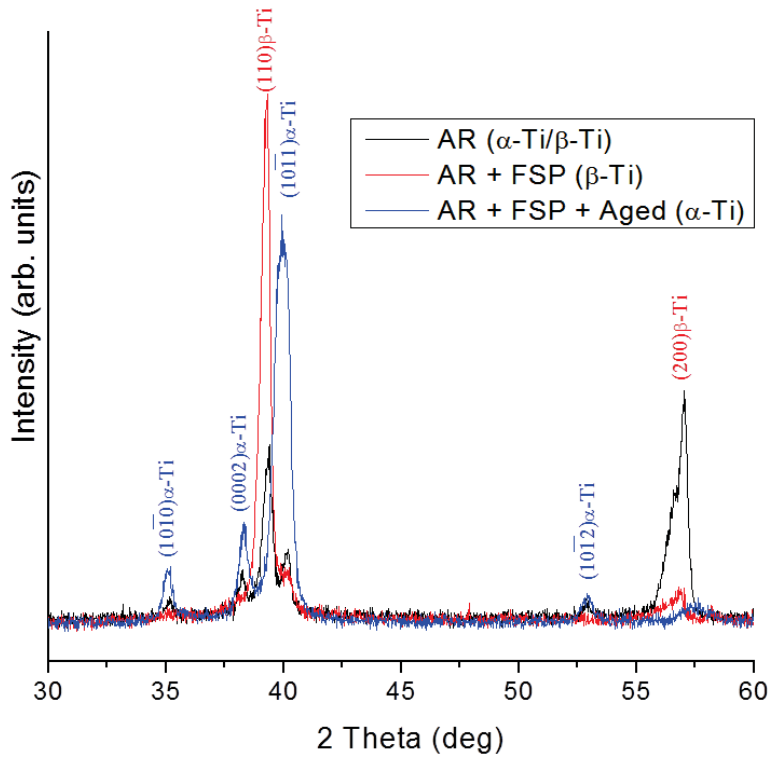

Figure 3.1. XRD scan of Ti-185 alloy in AR, FSP and Aged conditions.

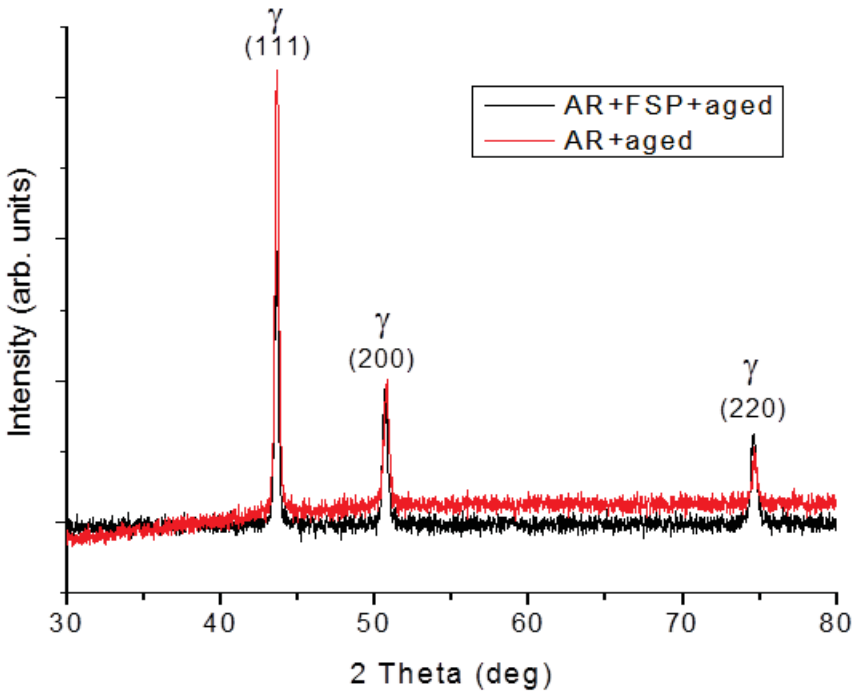

Figure 3.2. XRD scan of stainless steel A-286 alloy in AR, FSP and Aged conditions.

3.2 Vickers Micro-Hardness

Figure 3.3 and Figure 3.4 show the hardness cross-sectional profiles of Ti-185 alloys after friction stir processing, and hardening by water quenching (Aging), respectively. There was a slight increase in the Vickers micro-hardness of the AR+FSP sample in the stirred zone (SZ) compared to heat affected zone (HAZ), according to Figure 3.3. It shows an average hardness of

Figure 3.3. Vickers micro-hardness of AR+FSP Ti-185 alloy. SZ=Stir Zone, HAZ=Heat affected zone,

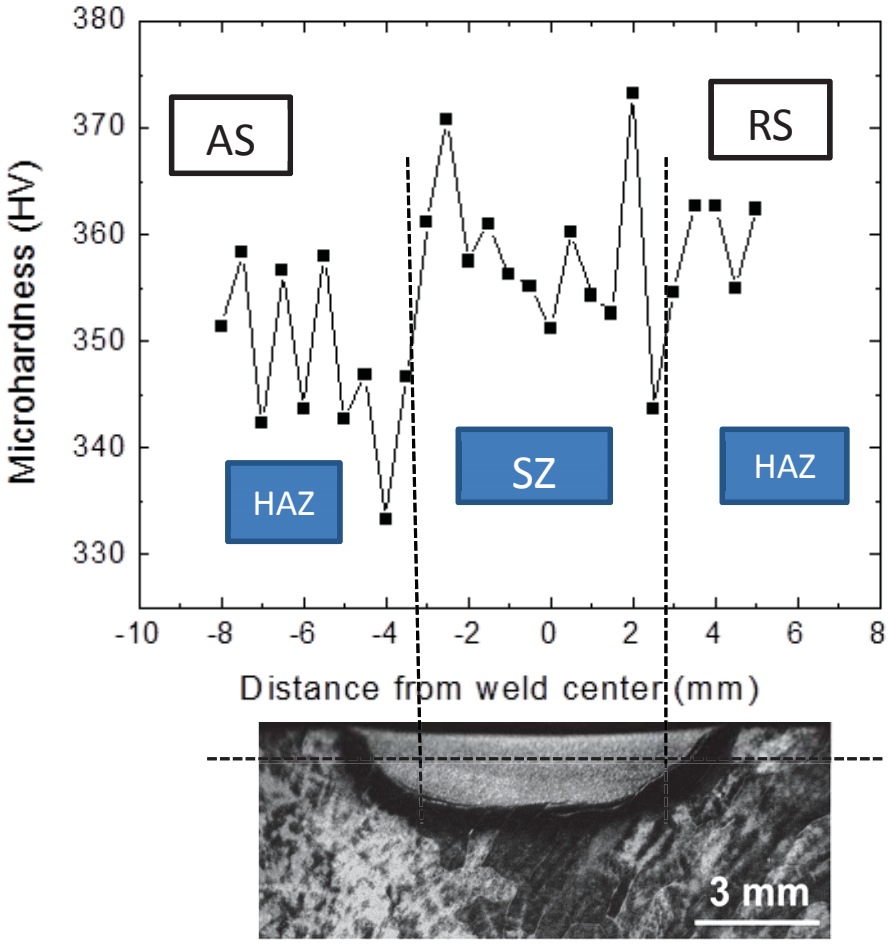

RS=Retreating side, AS=Advancing side. Result courtesy of V. Tungala (UNT).

360 ± 6 HV with a maximum value of 372 HV. For the AR+FSP+Aged sample in Figure 3.4, the Vickers mico-hardness increased more in the HAZ and SZ to an averaged value of 452 ± 6 HV with a highest hardness of about 461 HV. There was no further micro-hardness increase in the SZ compared to HAZ. The overall increase in hardness is expected with aging. The role of micro-hardness on the sliding wear properties will be discussed in the next section.

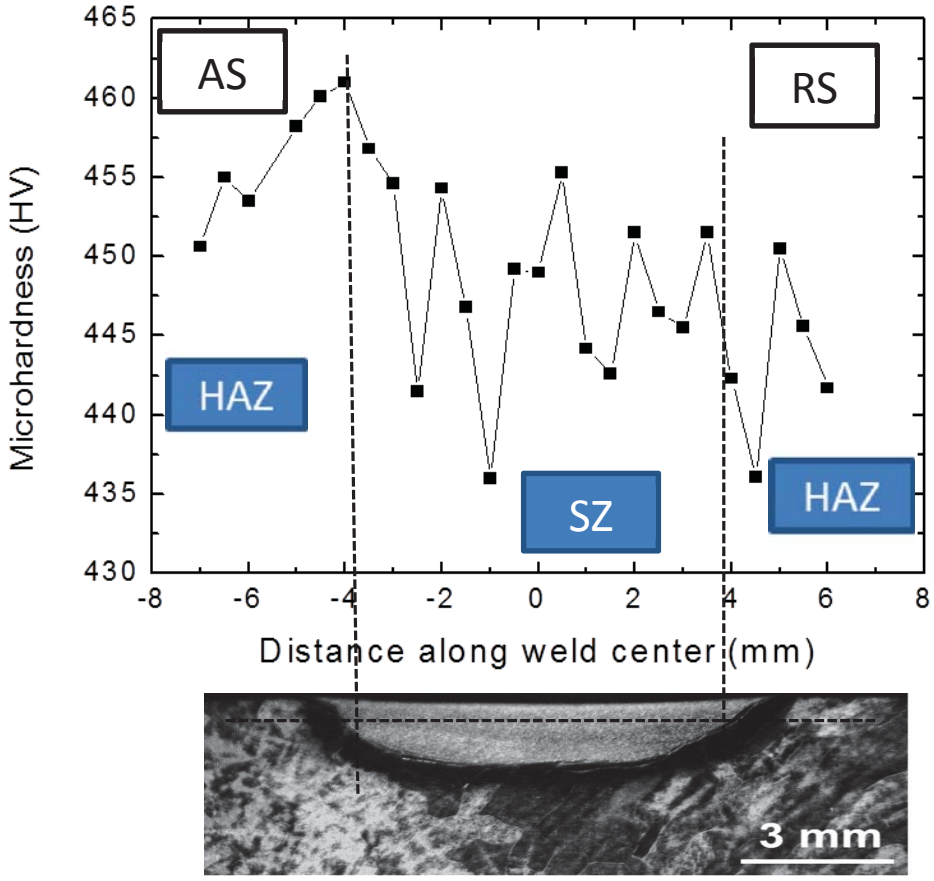

Figure 3.4. Vickers micro-hardness of AR+FSP+Aged Ti-185 alloy. SZ=Stir Zone, HAZ=Heat affected zone, RS=Retreating side, AS=Advancing side. Result courtesy of V. Tungala (UNT).

Figure 3.5 shows the Vickers micro-hardness cross-sectional profiles of the A-286 alloy after FSP and precipitation hardening (aging), via heat hardening by water quenching. The three curves represent the micro-hardness profiles acquired at three different distances of 2, 4, and 4.5 mm from the top edge of the sample. Clearly inside the SZ there are significant improvements in micro-hardness compared to HAZ and aged regions. The averaged hardness results within the SZ are summarized in the table 3.1.

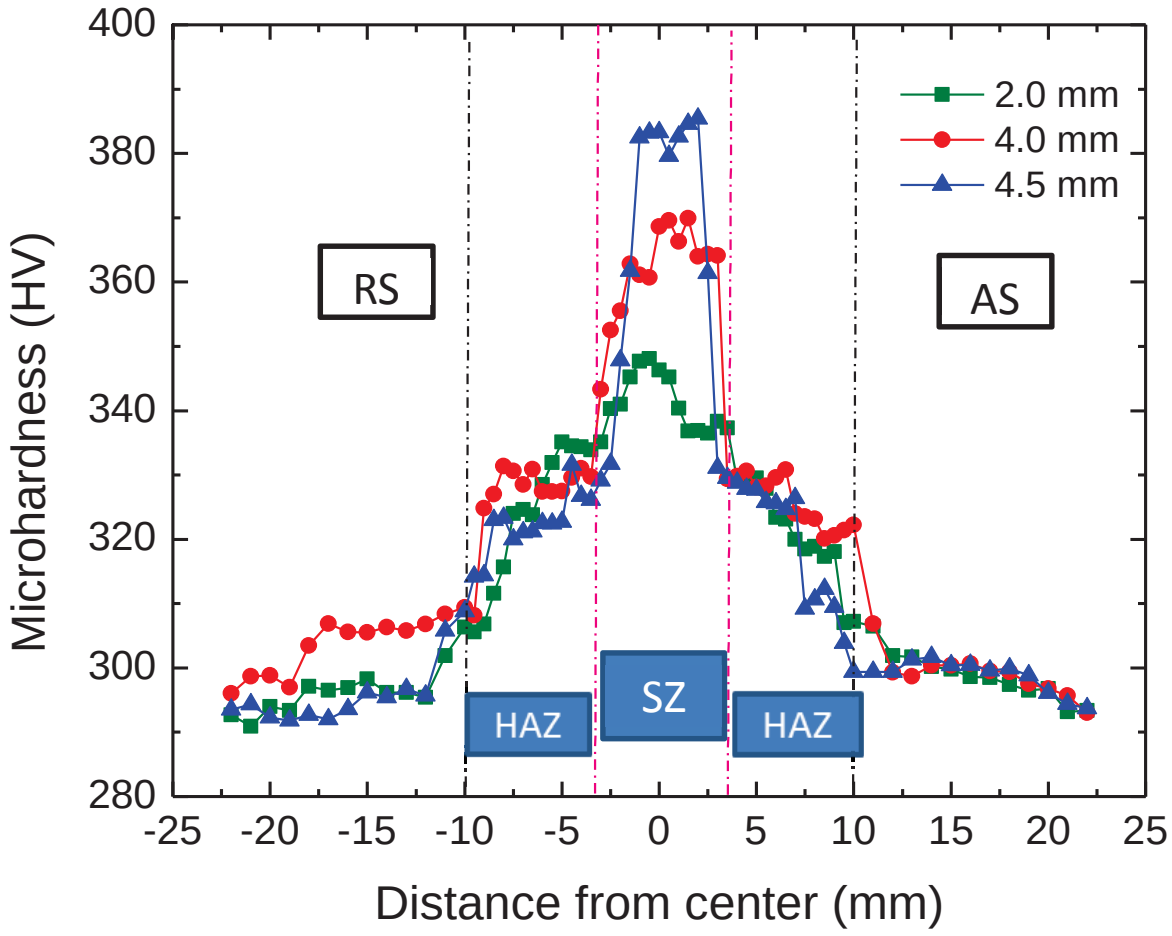

Figure 3.5. Vickers micro-hardness of AR+FSP+Aged A-286 alloy. SZ=Stir Zone, HAZ=Heat affected zone, RS=Retreating side, AS=Advancing side. Result courtesy of S. Das (UNT).

Table 3.1. Averaged Vickers micro-hardness (HV) values with standard deviations of stainless steel A-286 alloy based on Figure 3.5 data.

Sample	**Hardness (HV)**
AR+aged (Baseline)	295 ± 6
AR+FSP+aged (2mm)	348 ± 6
AR+FSP+aged (4mm)	368 ± 6
AR+FSP+aged (4.5mm)	385 ± 6

At all three depths, the A-286 alloy showed significant improvements in hardness after FSP. The results show that the greater the depth, the shallower the SZ and the greater the hardness of the alloy, which further means that hardness is dependent on depth. While the baseline hardness of the AR+aged alloy had already precipitation hardened, a further hardness increase due to FSP is attributed to grain refinement (Hall-Petch strengthening) and strain hardening in the SZ. This improvement in the micro-hardness is expected to reduce the sliding contact wear area under an applied load, and hence decrease the wear rate, which will be discussed in the next section.

3.3 Sliding Wear Behavior

Table 3.2 summarizes the HFRR sliding wear results for the Ti-185 alloy in AR, AR+FSP, and AR+FSP+Aged conditions. As expected, the larger the wear track depth and cross-sectional wear area removed, the higher the wear factor/rate. The AR+FSP+Aged alloy exhibited the lowest wear factor of 1.6 x 10^{-5} $mm^3/N \cdot m$, which is considered a relatively mild wear factor for a metallic alloy. As shown in section 3.1, XRD determined that this AR+FSP+Aged alloy exhibits the α-Ti phase whereas the AR+FSP alloy has the β–Ti phase. Therefore, the high wear rate of AR+FSP alloy is likely due to predominance of this β–Ti phase with FSP-induced (110) texture, since β–Ti is known to be softer and more compliant compared to α-Ti. Furthermore, this (110) texture is not conducive to low sliding wear factor. In contrast, the AR+FSP+Aged alloy with β-phase decomposition has the harder and stiffer α-Ti present, hence lowest wear rate. In comparison, Ti-6Al-4V (α/β Ti alloy) without FSP has a wear rate typically around 2x10^{-4} $mm^3/N \cdot m$ [1], an order of magnitude higher wear rate than these Ti-185 alloys.

Table 3.2. Summary of averaged wear track depth, cross-sectional wear area removed, and wear factor for Ti-185 alloys in AR, AR+FSP, and AR+FSP+Aged conditions (with denoted Ti phase(s) present).

Alloy (Ti phase)	**Wear track depth (μm)**	**Wear area (μm^2)**	**Wear factor ($mm^3/N \cdot m$)**
AR (α/mostly β)	5.5 ± 0.7	896 ± 158	2.1 x 10^{-5}
AR+FSP (β textured 110)	8.8 ± 1.0	2187 ± 365	5.1 x 10^{-5}
AR+FSP+Aged (α)	5.1 ± 0.9	672 ± 133	1.6 x 10^{-5}

After sliding, optical microscopy images were acquired to examine the surface wear morphology and debris on the Ti-185 alloy wear tracks and mating Si_3N_4 sliding counterface balls. Figure 3.6 shows the worn images for AR+FSP+Aged (a,b) and AR+FSP (c,d) Ti-185 alloys where the Si_3N_4 ball surface and the wear tack of the AR+FSP+aged alloy exhibit slightly lower wear contact area and less debris compared to the AR+FSP alloy. Therefore, the lower wear values listed in Table 3.2 for AR+FSP+Aged alloy. This can be attributed to the higher micro-hardness values with aging, shown previously in Figure 3.4. The wear surfaces in Figure 3.6 show evidence of micro-abrasive wear.

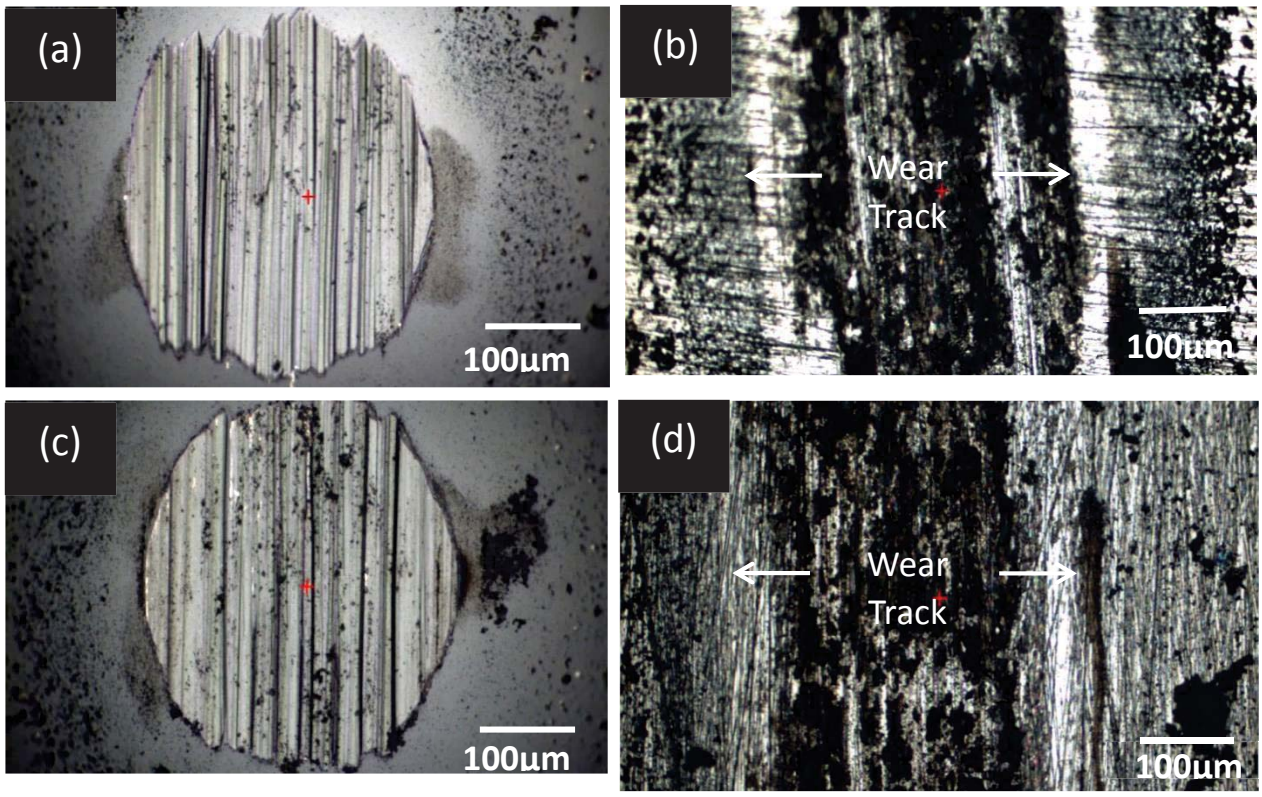

Figure 3.6. Optical microscopy images after HFRR testing of (a) Si_3N_4 ball sliding on (b) Ti-185 (AR+FSP+Aged) wear track, and (c) Si_3N_4 ball sliding on (d) Ti-185 (AR+FSP) wear track.

Table 3.3 summarizes the HFRR sliding wear results for the stainless steel A-286 alloy in AR+Aged and AR+FSP+Aged conditions. FSP results in improving all wear values listed in Table 3.3. A wear factor of 5.8 x 10^{-7} $mm^3/N \cdot m$ for the AR+FSP+Aged alloy is considered a very low wear factor when compared to untreated metallic alloys. These values are also substantially lower than the Table 3.2 wear values for the Ti-185 processed alloys, implying the AR+FSP+Aged stainless steel A-286 alloy is more wear resistant than the AR+FSP+Aged Ti-185 alloy. This can be attributed in part to the increased micro-hardness in the SZ, shown previously in Figure 3.5. However, these hardness values (368 HV) are still lower than the Ti-185 alloy values in Figure 3.4 (452 HV), suggesting that hardness along is not entirely responsible for improvements in the sliding wear behavior. Therefore, the microstructure and microstructural evolution during FSP and sliding wear are additionally responsible for the improvement in A-286 wear resistance, and will be discussed in the next sections.

Table 3.3. Summary of averaged wear track depth, cross-sectional wear area removed, and wear factor for stainless steel A-286 alloys in AR+aged and AR+FSP+Aged conditions.

Alloy	Wear track depth (μm)	Wear area (μm^2)	Wear factor ($mm^3/N \bullet m$)
AR+aged	0.52 ± 0.13	44 ± 17	1.0 x 10^{-6}
AR+FSP+Aged (4.0 mm)	0.45 ± 0.12	24 ± 9	5.8 x 10^{-7}

After sliding, optical microscopy images were acquired to examine the surface wear morphology and debris on the A-286 alloy wear tracks and mating Si_3N_4 sliding counterface balls. Figure 3.7 shows the worn images for AR+FSP+Aged (a,b) and AR+Aged (c,d) A-286 alloys where the Si_3N_4 ball surface and the wear tack of the AR+FSP+aged alloy exhibit lower wear contact area and much less abrasive debris compared to the AR+Aged alloy.

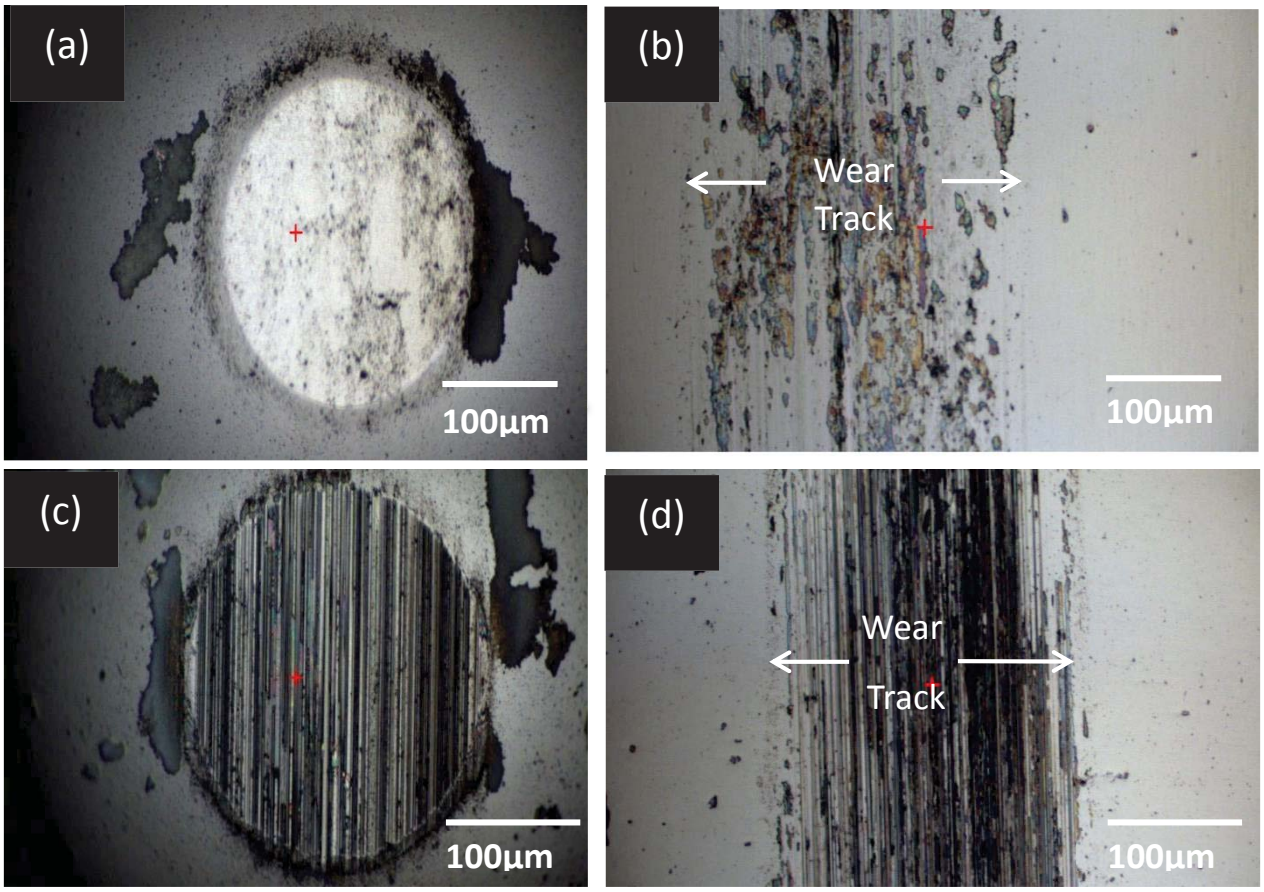

Figure 3.7. Optical microscopy images after HFRR testing of (a) Si_3N_4 ball sliding on (b) A-286 (AR+FSP+Aged) wear track, and (c) Si_3N_4 ball sliding on (d) A-286 (AR+Aged) wear track.

In addition to optical microscopy, SEM imaging was conducted on the A-286 wear tracks to determine with higher and better surface resolution the differences in optical images in Figure 3.7 (b,d). Figure 3.8 compares the SEM images of the wear tracks of the A-286 alloy in (a) AR+Aged and (b) AR+FSP+Aged conditions. Clearly the wear track SEM morphologies are different: increased coarse abrasion (galling) with AR+Aged alloy and finer-scale abrasion with AR+FSP+Aged alloy. Hence, the wear debris is larger for AR+Aged alloy, confirming the

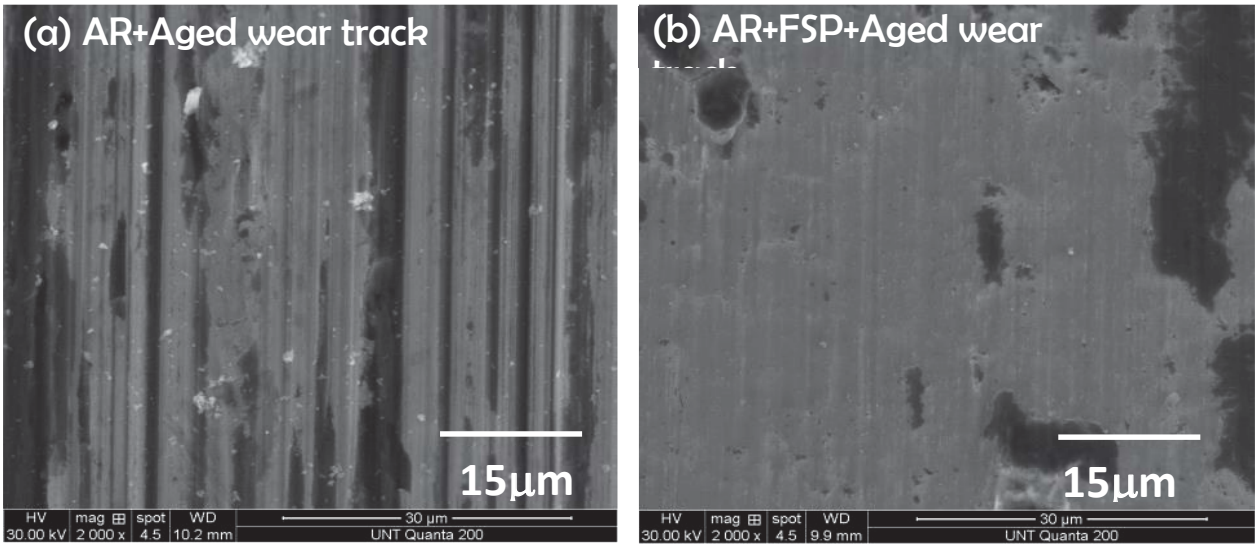

Figure 3.8. SEM images of A-286 alloys after HFRR testing of (a) AR+Aged and (b) AR+FSP+Aged wear tracks.

observations based on the optical images in Figure 3.7. This clearly shows why the AR+FSP+Aged alloy has a shallower wear depth, wear area and lower wear factor compared to AR+Aged alloy. However, the mechanism behind such wear behavior needs further investigation and will be determined with cross-sectional FIB microscopy discussed now.

3.4 Wear Mechanisms

In order to account for the differences in the wear results and behavior above, more detailed, advanced characterization techniques are needed, such as cross-sectional FIB-SEM. Such microscopy studies of the cross-sections inside and outside the wear tracks were acquired after HFRR testing to determine the microstructural evolution during wear for both AR+Aged and AR+FSP+Aged A-286 alloys. Figure 3.9 shows FIB-SEM cross-sectional image of the AR+FSP+Aged A-286 alloy inside the FSP SZ (outside the wear track). Clearly there is FSP-

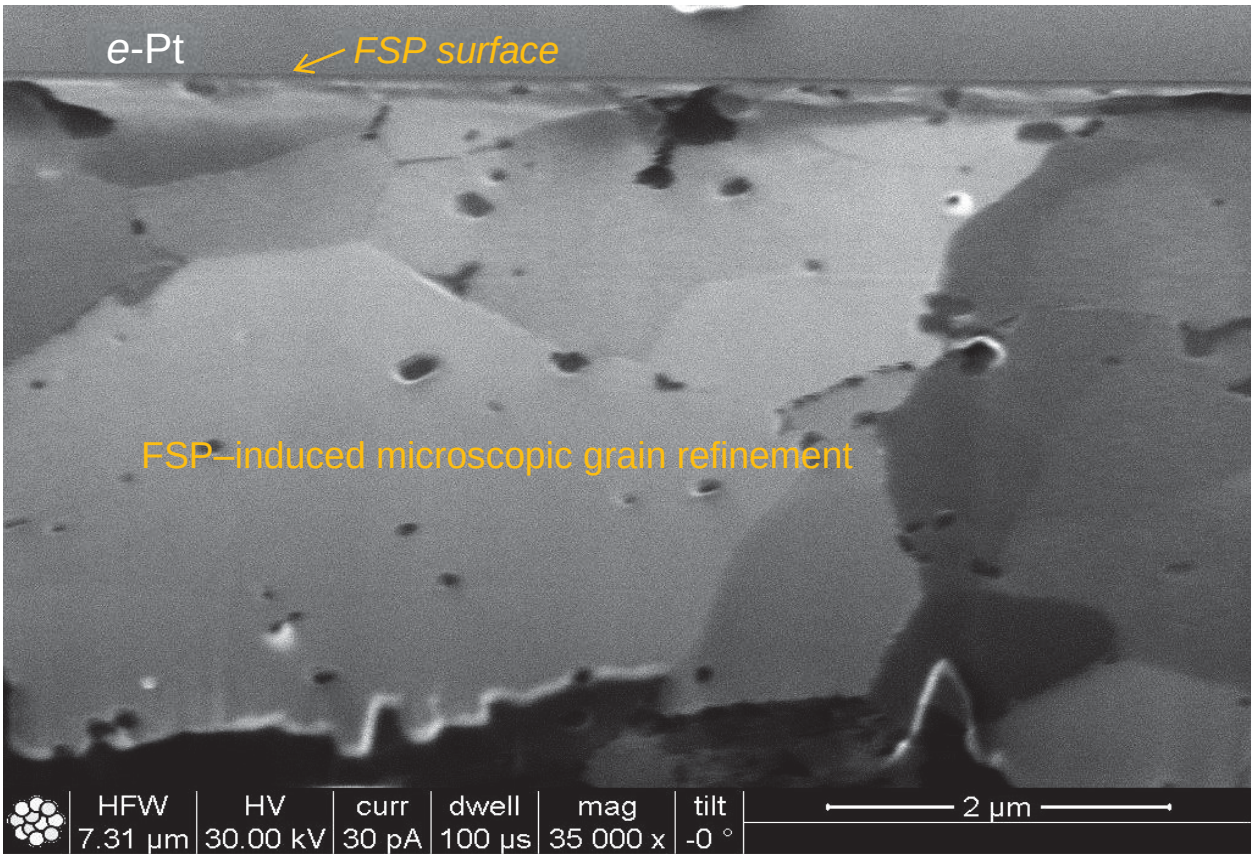

Figure 3.9. FIB-SEM image of AR+FSP+Aged A-286 alloy inside FSP SZ, 4.0 mm depth (outside the wear track).

induced microscopic grain refinement to a finer scale depth of ~2 µm and coarser size depth below it. This grain refinement is responsible for the increase in hardness shown in Figure 3.5 via Hall-Petch strengthening.

Figures 3.10 to 3.12 show a series of low to higher magnification FIB-SEM images of same alloy AR+FSP+Aged A-286 alloy, but now inside the wear track shown previously in Figure 3.8(b). This wear track was generated on the FSP SZ shown in Figure 3.9.

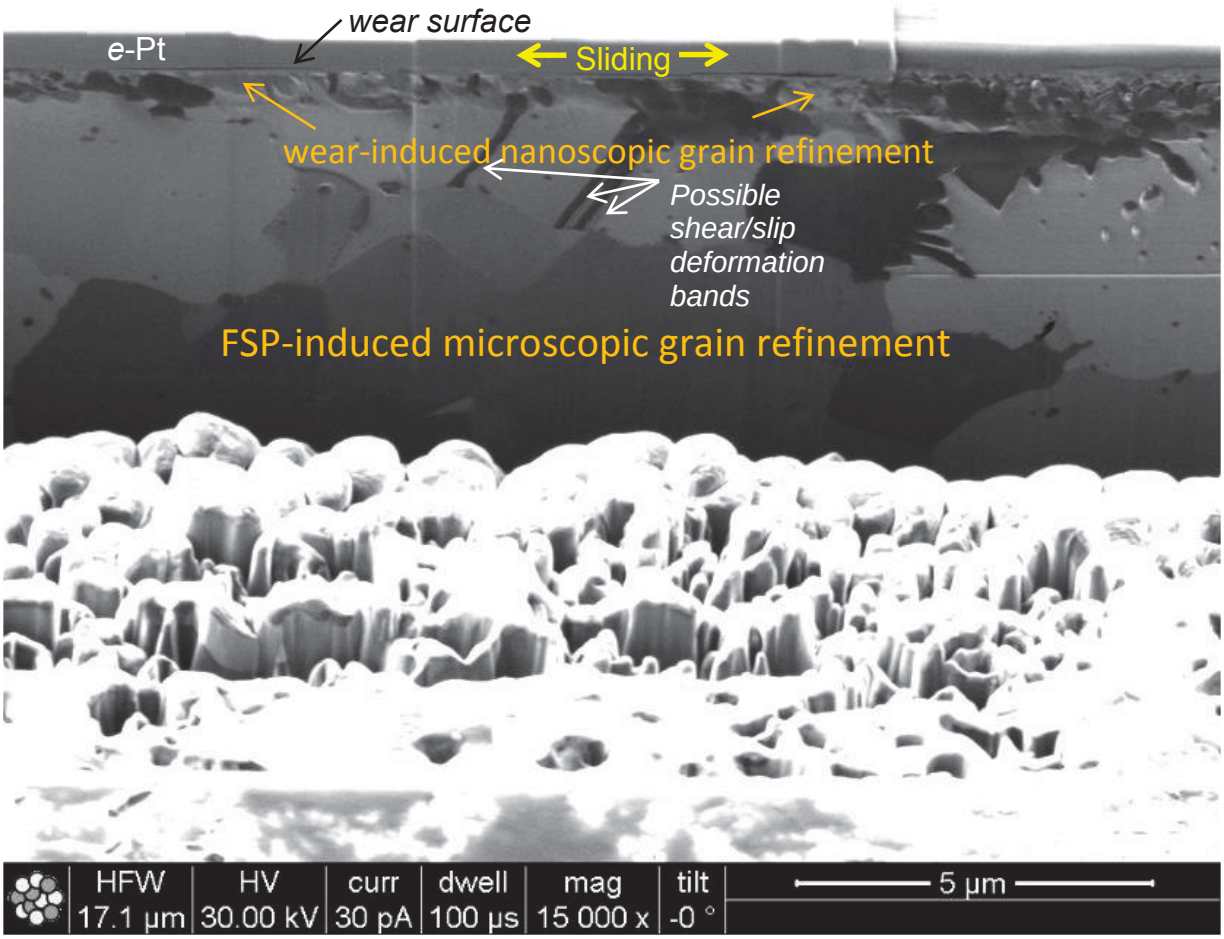

Figure 3.10. Low magnification FIB-SEM image of AR+FSP+Aged A-286 alloy inside wear track on FSP SZ.

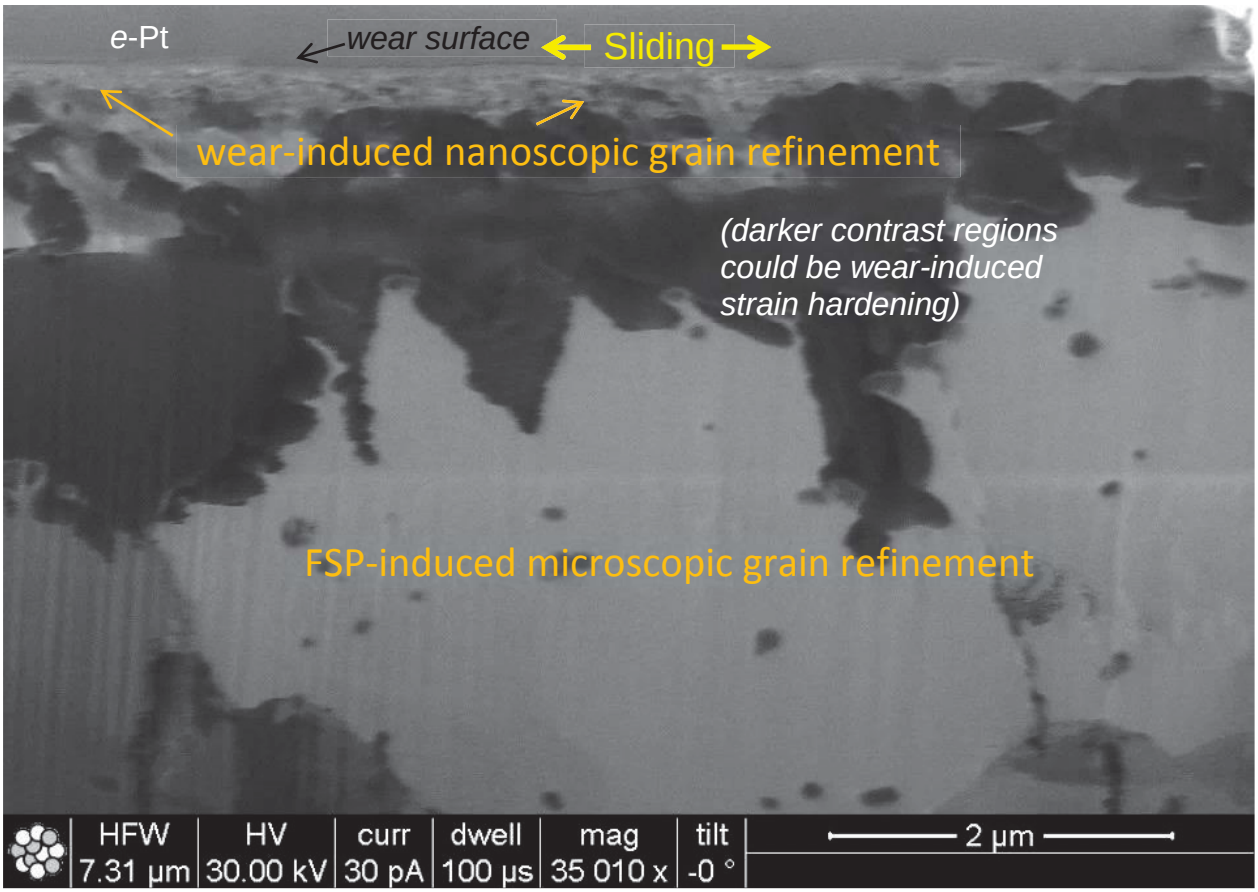

Figure 3.11. Higher magnification FIB-SEM image of AR+FSP+Aged A-286 alloy inside wear track on FSP SZ.

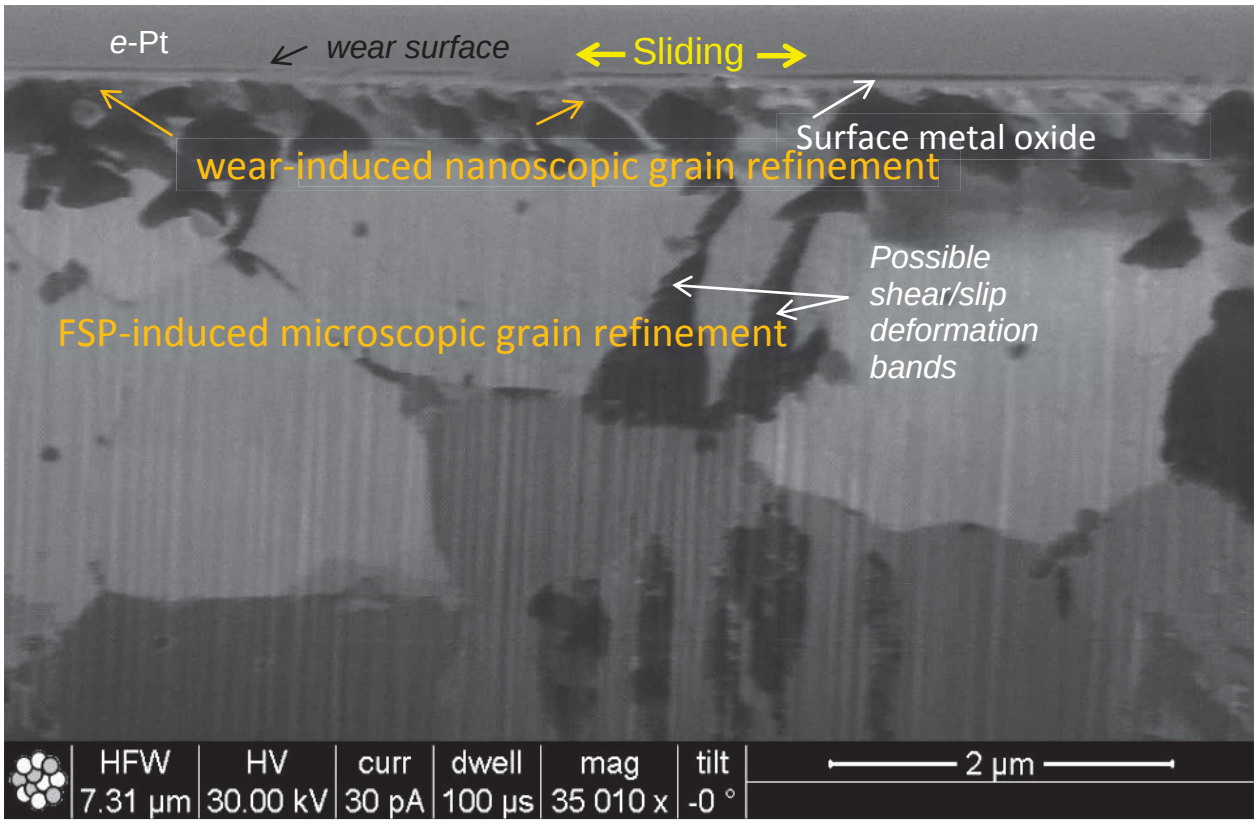

Figure 3.12. Higher magnification FIB-SEM image of AR+FSP+Aged A-286 alloy inside wear track on FSP SZ.

Based on the cross-sectional FIB-SEM images in Figures 3.10, 3.11, and 3.12, there is an additional sliding wear-induced nanoscopic grain refinement region that could further lead to increased strength and hardness. The enhanced hardness of FSP reduced the extent of abrasion when comparing the AR+FSP+Aged alloy to AR+Aged alloy (Figure 3.8). The nanoscopic and microscopic grain refinement resulting from wear and FSP, respectively, reduced the level of damage and surface fatigue wear. This accounts for the lowest wear factor of the AR+FSP+Aged alloy. Therefore, hardness alone is not solely responsible for improved wear resistance but also this wear-induced nanostructural grain refinement evolution mitigates wear. In addition, subsurface wear-induced strain hardening and shear/slip deformation bands, shown in Figure 3.11 and Figure 3.12, respectively, could also result in improved wear resistance. Micro-

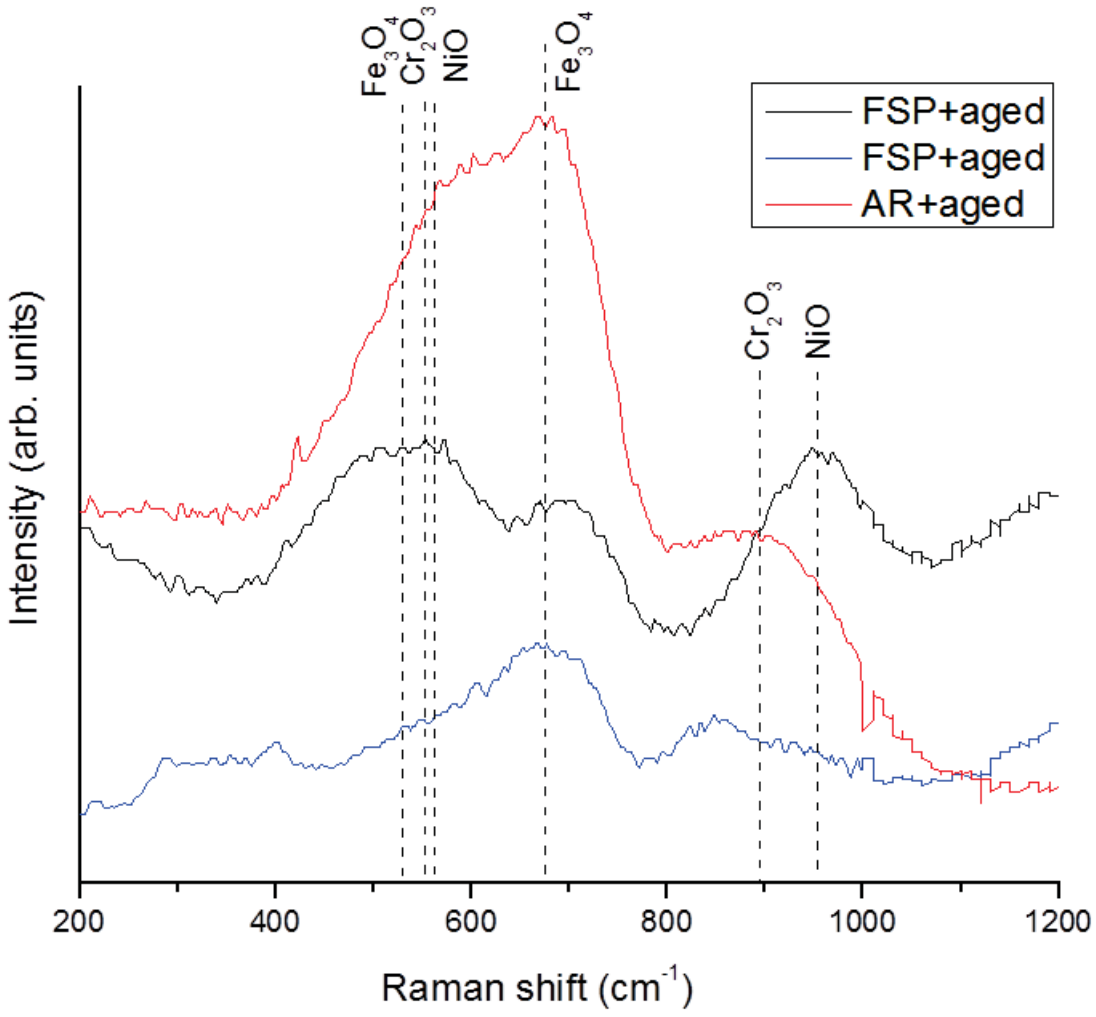

Figure 3.13. Micro-Raman spectroscopy of surface metal oxides on AR+Aged and AR+FSP+Aged A-286 alloy inside wear track on FSP SZ shown in Figure 3.12.

Raman spectroscopy inside the stir wear zone determined that the very thin wear debris contained metal oxides of Fe_3O_4, Cr_2O_3, and NiO (Figure 3.13). In addition, Scanning Auger microscopy/spectroscopy in Figure 3.14 revealed some areas, e.g. labeled area 1, of the wear track also contained silicon oxide wear debris transferred from the worn sliding Si_3N_4 counterface. Although these metal oxides and silicon oxide wear debris makes up a small

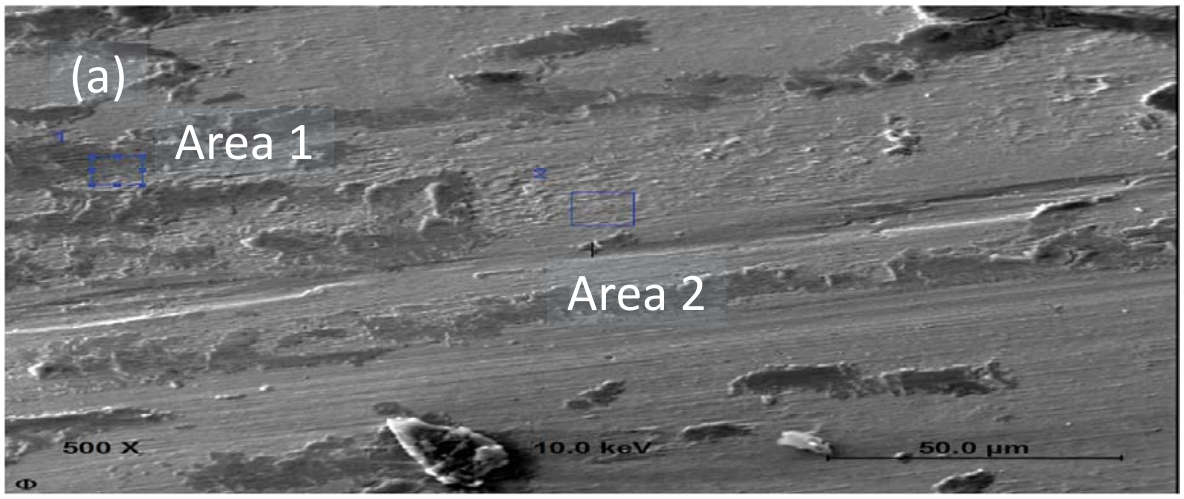
(a)
Area 1
Area 2
500 X
10.0 keV
50.0 µm

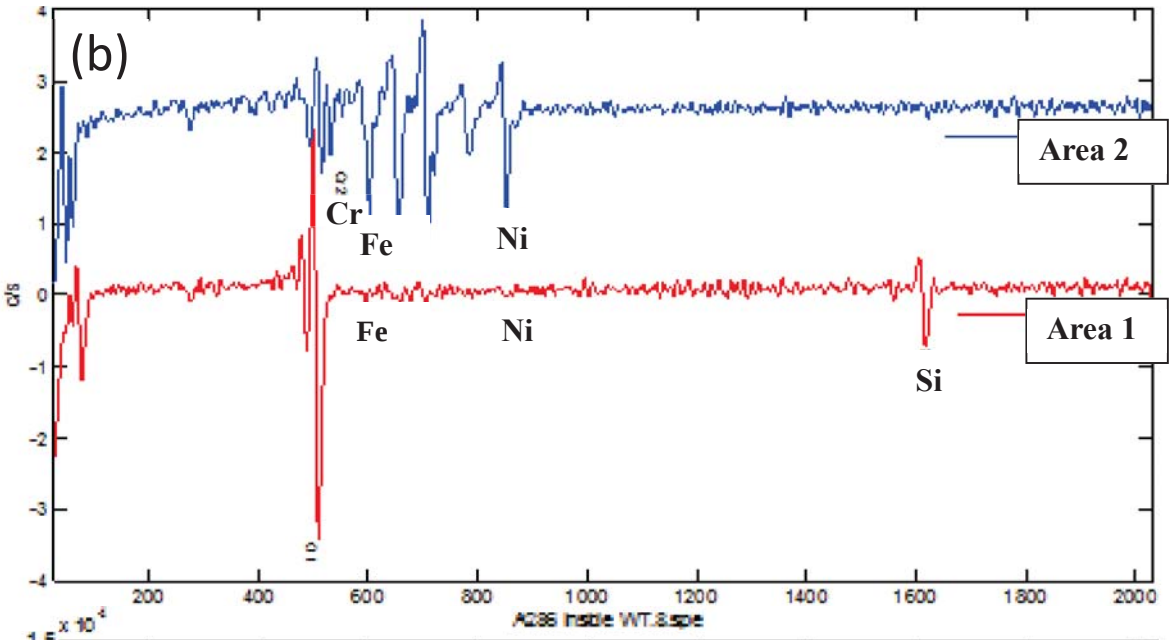
(b)
Area 2
Area 1
Cr
Fe
Ni
Fe
Ni
Si
A286 Inside WT.Espe

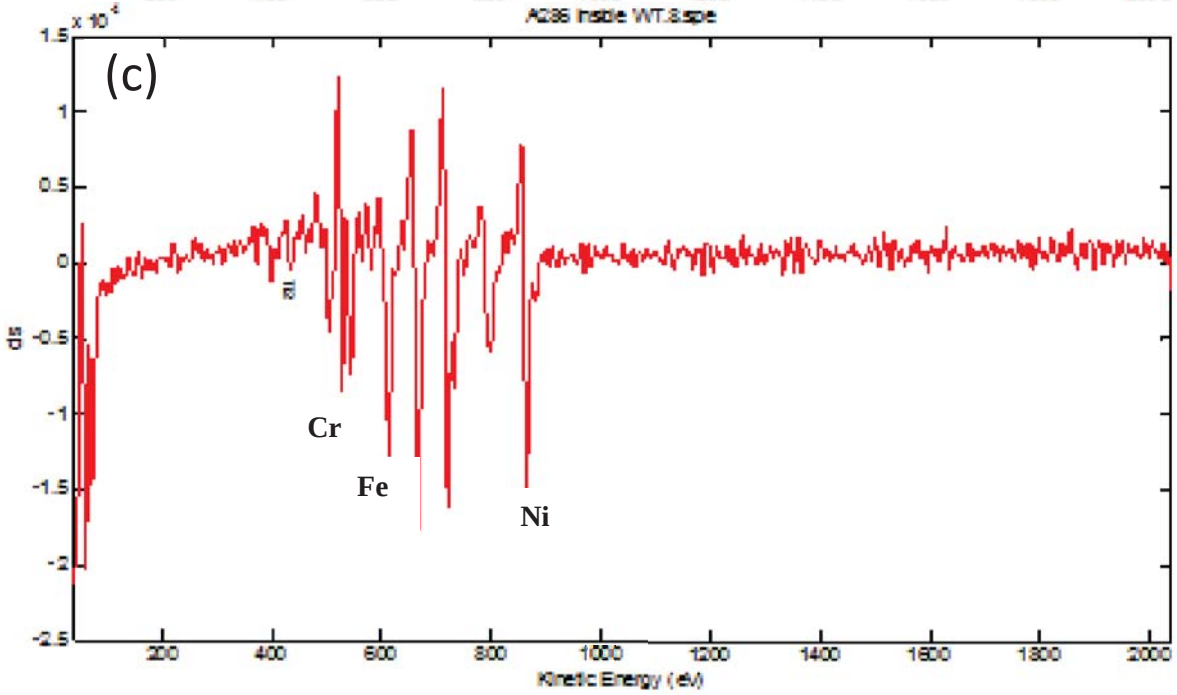
(c)
Cr
Fe
Ni
Kinetic Energy (eV)

Figure 3.14. (a) Auger secondary electron image and corresponding Auger spectroscopy scan of surface metal oxides on AR+FSP+Aged A-286 alloy (b) inside wear track on FSP SZ shown in Figure 3.12 showing two different Areas 1 and 2 inside the wear track. (c) Bottom scan is acquired outside the wear track in FSP SZ.

portion of the wear track contact area, and thus is a consequence and not the cause of low wear rates. The Auger spectra in Figure 3.14(b) reveal the presence of oxides of chromium, iron, nickel and silicon inside the wear track area 1, but no oxides are present in wear track area 2. The Auger spectra acquired outside the wear track area in Figure 3.14(c) also reveals no oxides, just the major constituent metals in the A-286 alloy.

Figure 3.15 shows a FIB-SEM image of AR+Aged A-286 alloy outside the wear track, which shows there is no FSP-induced microscropic grain refinement, and hence there is lower hardness and higher wear factor reported earlier. The absence of elevated hardness increased the extent of abrasion, when comparing the Figure 3.8 surface wear track morphologies that showed AR+Aged exhibited increased micro-abrasion. Without the benefits of FSP-induced grain refinement, there is an increased level of damage and surface fatigue wear. Figures 3.16 and 3.17 shows FIB-SEM images inside the wear tracks that shows little to no wear-induced nanostructural grain refinement with AR+Aged sample that further translates to higher wear factors. There is some darker contrast regions likely due to wear-induced strain hardening; however, without the FSP-induced and wear induced microscopic and nanoscopic grain refinement, there is lower hardness and increased abrasive wear.

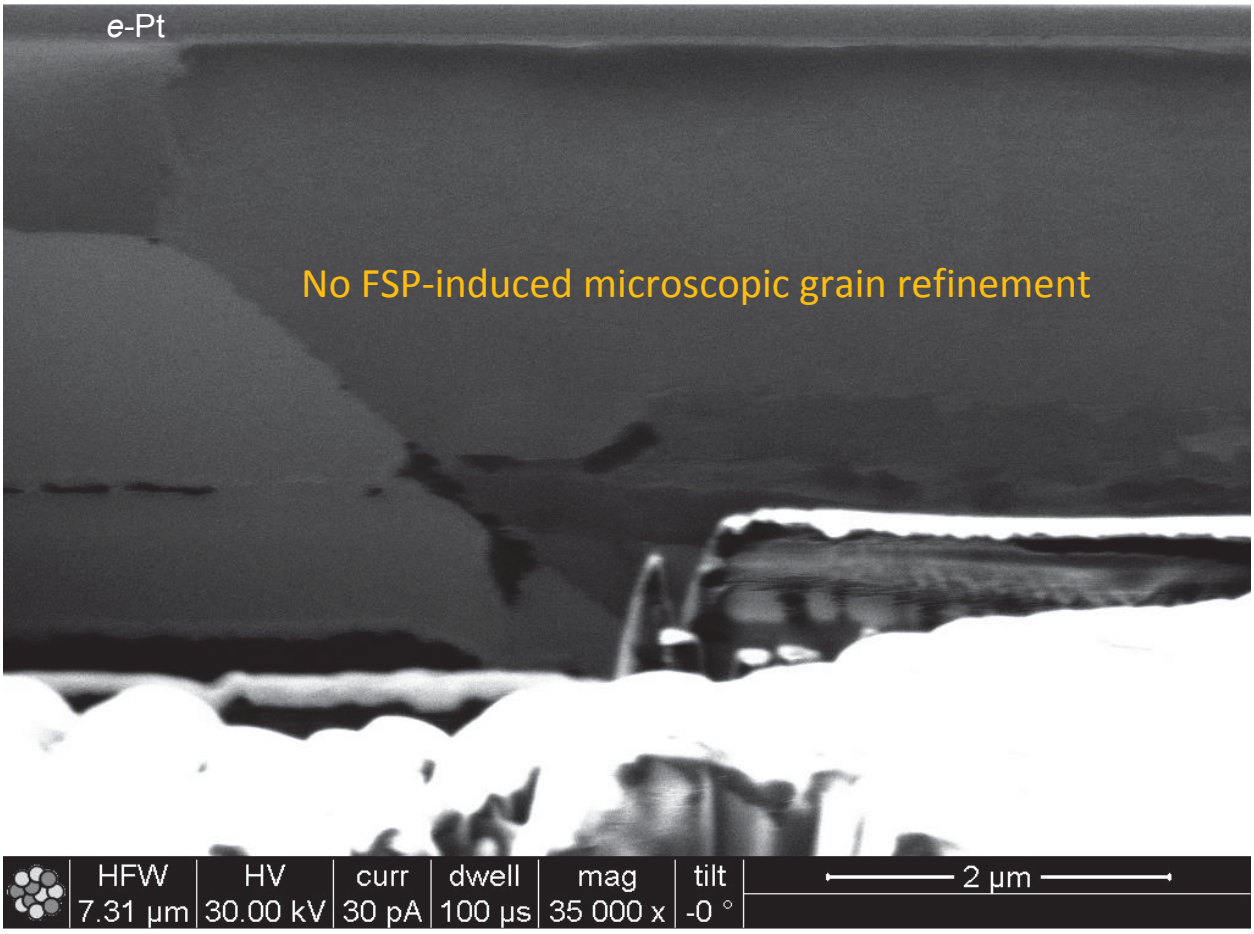

Figure 3.15. FIB-SEM image of AR+Aged A-286 alloy outside the wear track.

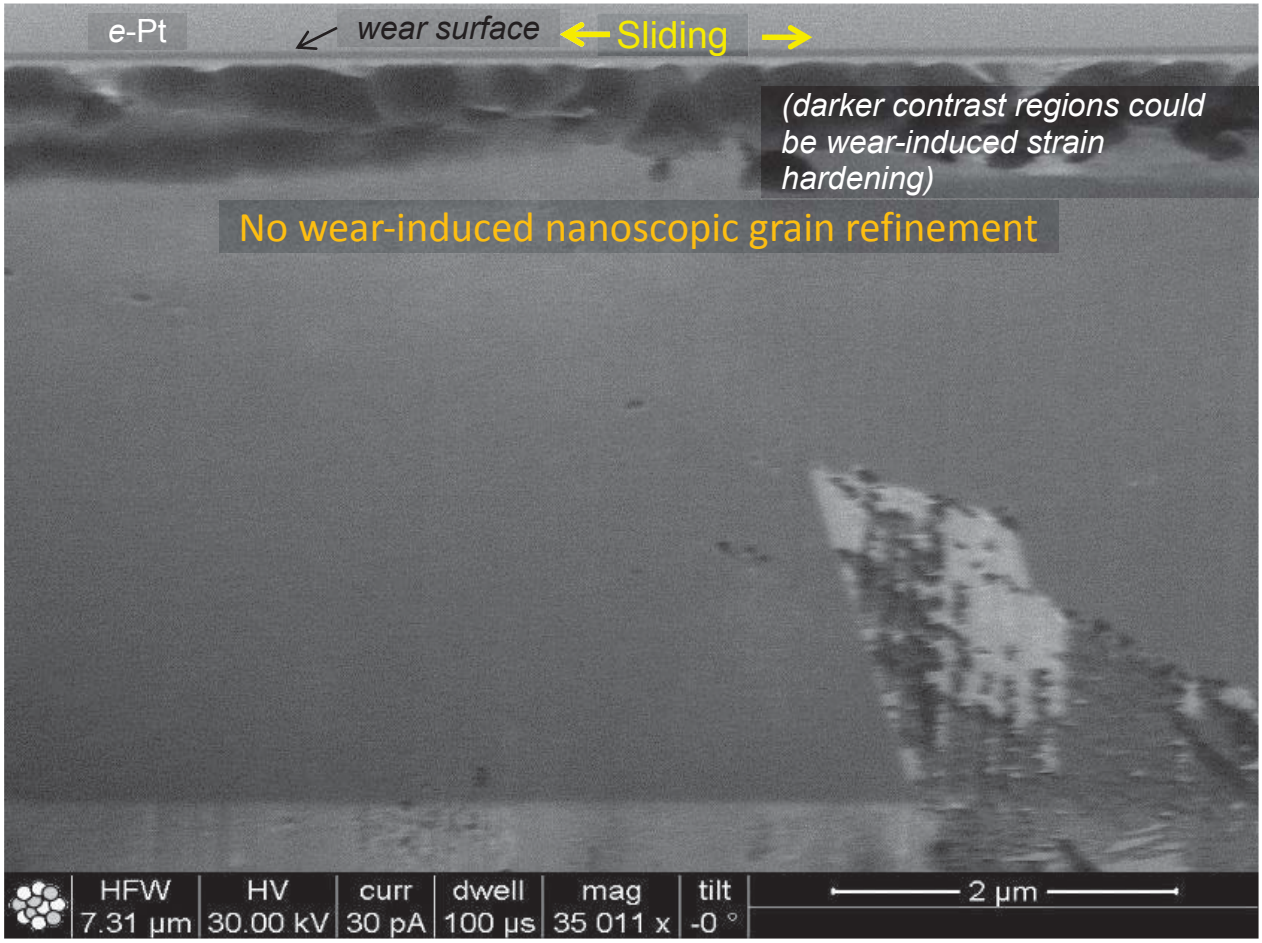

Figure 3.16. FIB-SEM image of AR+Aged A-286 alloy inside the wear track.

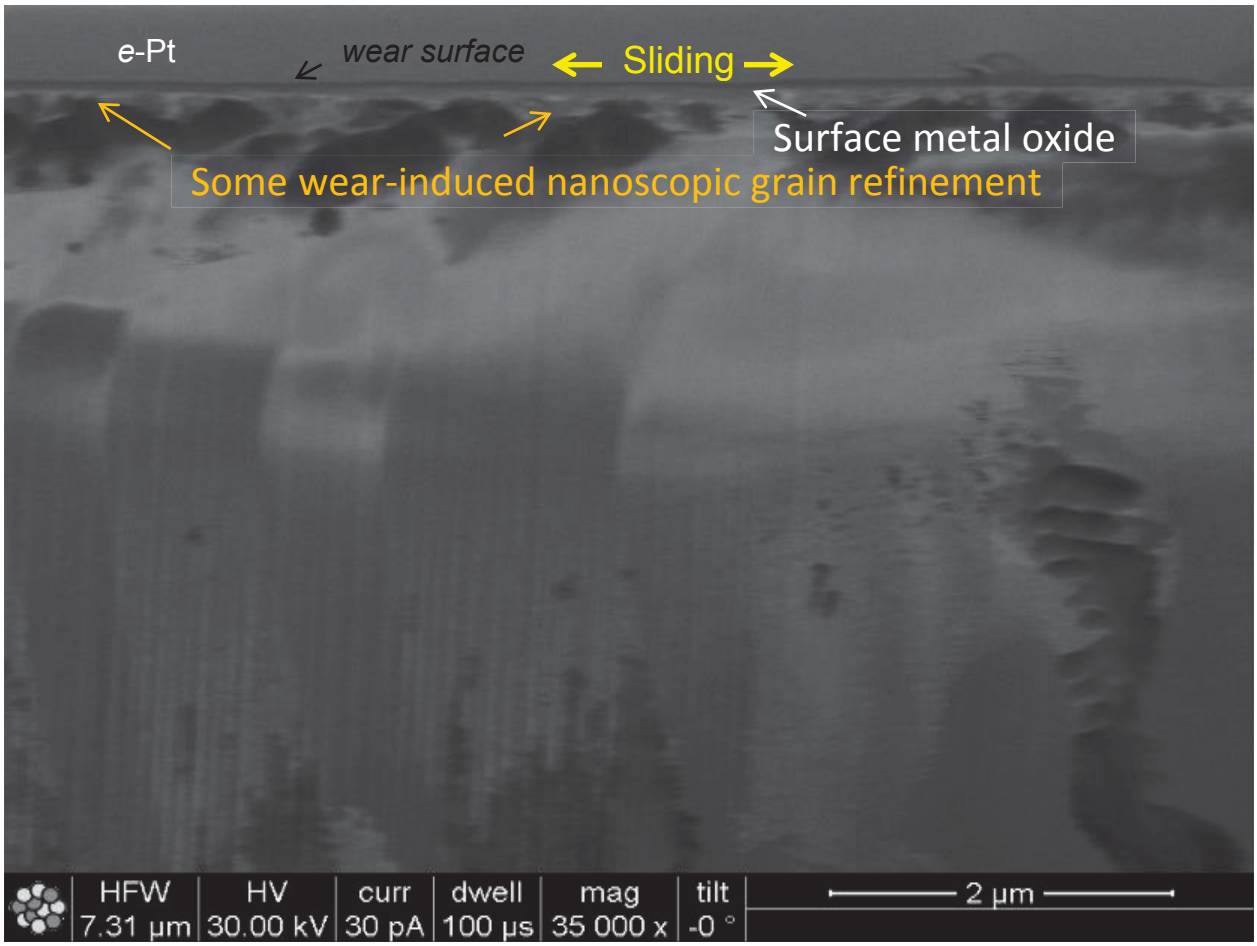

Figure 3.17. FIB-SEM image of AR+Aged A-286 alloy inside the wear track.

CHAPTER 4

SUMMARY AND CONCLUSIONS

This study investigated the effect of friction stir processing on the wear behavior of titanium (Ti-185) and stainless steel (A-286) alloys. Friction stir processing was used as a surface engineering technique for microstructural modification of these alloys with the aim to increase hardness and decrease wear rate. In addition to measuring these mechanical and tribological properties, fundamental mechanisms responsible for such behavior were determined using focused ion beam/scanning electron microscopy, x-ray diffraction, Raman spectroscopy, and scanning Auger microscopy/spectroscopy inside stir zones and wear tracks. Based on the experimental results and characterization analyses, the following conclusions were determined for Ti-185 and A-286 alloys processed in different conditions (AR, AR+aged, AR+FSP, or AR+FSP+Aged).

- Overall, the AR+FSP+aged condition alloys exhibited the best wear resistance (lowest wear rates achieved of 1.6×10^{-5} and 5.8×10^{-7} $mm^3/N \cdot m$ for Ti-185 and A-286 alloys, respectively). Compared to non-FSP alloys, these values were about a half magnitude order of improvement.
- In part, the increasing micro-hardness in the stir zone due to FSP-induced microscopic grain refinement was responsible for decreasing wear rates. In contrast, the absence of FSP-induced grain refinement resulted in lower hardness, and hence increasing wear rate.
- Further improvement in the wear resistance of A-286 alloy was due to wear-induced nanostructural grain refinement/Hall-Petch strengthening.
- For the Ti-185 alloy, x-ray diffraction revealed that there was a phase transformation from β-Ti (AR+FSP) to α-Ti (AR+FSP+aged). This β-phase decomposition resulted in the harder and stiffer α-Ti phase responsible for lowering of wear rate in Ti-185.

- For the A-286 alloy, there was increased coarse abrasion (galling) with the AR+aged alloy compared to the much finer-scale abrasion with the AR+FSP+aged alloy, which was responsible for smaller and less abrasive wear debris, and hence lower wear rate.
- Micro-Raman spectroscopy inside the stir wear zone determined that the wear debris contained metal oxides of Fe_3O_4, Cr_2O_3, and NiO. Scanning Auger microscopy/ spectroscopy revealed some areas of the wear track also contained silicon oxide wear debris transferred from the worn sliding Si_3N_4 counterface, although this wear debris makes up a small portion of the wear track contact area, and thus is a consequence and not the cause of low wear rates.

Overall, friction stir processing of titanium and stainless steel alloys resulted in lowering of wear rates suggesting it is a viable surface engineering technique to mitigate and target site-specific wear.

CHAPTER 5

FUTURE WORK

This study shows that FSP is a viable technique for microstructural modifications to improve hardness and wear resistance. The following points are recommended areas to further build on this work for A-286 and Ti-185 alloys.

- More experimental FSP on investigating the effect of tool design on the resulting microstructure.
- Fretting-type wear tests should be carried out at higher temperatures to determine thermal stability limit and effect on wear rate.
- Load/contact stress dependent wear tests should be conducted to determine their effect on wear rates.
- Other relevant mechanical properties, such as ductility and fracture toughness, should be measured to determine if they influence wear rates.
- More chemical spectroscopy and transmission electron microscopy/electron diffraction needs to be conducted on the FIB cross-sections inside the stir zones and wear tracks to determine the difference in phase contrasts observed in A-286 alloy.

REFERENCES

[1] R.S. Mishra, Z.Y. Ma, Friction stir welding and processing, Mater. Sci. Eng. R 50, 1 (2005).

[2] R.S. Mishra, P. Sarathi De, N. Kumar, Friction stir welding and processing, Science and Engineering, Springer, New York, New York, 2014.

[3] C. Lorenzo-Martin, O.O. Ajayi, Rapid surface hardening and enhanced tribological performance of 4140 steel by friction stir processing, to appear on Wear, 2015.

[4] S.H. Aldajaha, O.O. Ajayi, G.R. Fenske, S. David, Effect of friction stir processing on the Tribological performance of high carbon steel, Wear 267 (2009) 350–355.

[5] N. Sun and D. Apelian, Friction stir processing of aluminum cast alloys for high performance applications, (2011) 44-60.

[6] R. Li, T. Yuan, Z. Qiu, K. Zhou, J. Li, Nanostructured Co–Cr–Fe alloy surface layer fabricated by combination of laser clad and friction stir processing, Surface & Coatings Technology 258 (2014) 415–425.

[7] B. Li, Y. Shen, W. Hu, L. Luo, Surface modification of Ti–6Al–4V alloy via friction-stir processing: Microstructure evolution and dry sliding wear performance, Surface & Coatings Technology 239 (2014) 160–170.

[8] A. Rahbar-kelishami, A. Abdollah-zadeh, M.M. Hadavi, R.A. Seraj, A.P. Gerlich, Improvement of wear resistance of sprayed layer on 52100 steel by friction stir processing, Applied Surface Science 316 (2014) 501–507.

[9] H.S. Arora, H. Singh, B.K. Dhindaw, Wear behavior of a Mg alloy subjected to friction stir processing, Wear 303 (2013) 65–77.

[10] S. Dodds, A.H. Jones, S. Cater, Tribological enhancement of AISI 420 martensitic stainless steel through friction-stir processing, Wear 302 (2013) 863–877.

[11] M.W. Mahoney, S.P. Lynch, Friction stir processing, OMB No. 0704-0188, 2006.

[12] J.F. Archard, Contact and rubbing of flat surfaces, Journal of applied physics, 24, 981-988, 1953

[13] S. Samuel, S. Nag, T.W. Scharf, and R. Banerjee, Wear resistance of laser-deposited boride reinforced Ti-Nb-Zr-Ta alloy composites for orthopedic implants," Materials science and engineering C: Biomimetic materials, sensors and systems, 28, 414-420 (2008).

[14] S.N. Dahotre, H.D. Vora, R.S. Rajamure, L. Huang, R. Banerjee, W. He, N.B. Dahotre, Laser induced nitrogen enhanced titanium surfaces for improved osseo-integration, Annals of biomedical engineering 42, 50-61, 2014.

[15] G. Purcek, O. Saray, O. Kul, I. Karaman, G.G. Yapici, M. Haouaoui, H.J. Maier, Mechanical and wear properties of ultrafine-grained pure Ti produced by multi-pass equal-channel angular extrusion, Materials science and engineering A 517 (2009) 97–104.

[16] I. Halevy, G. Zamir, M. Winterrose, G. Sanjit, Carlos Roberto Grandini, Ariel Moreno-Gobbi, Crystallographic structure of Ti-6Al-4V, Ti-HP and Ti-CP under high-pressure, Journal of physics: Conference series 215 (2010) 012013

[17] Soheyl Soleymani, Amir Abdollah-zadeh, and Sima Ahmad Alidokht, Improvement in tribological properties of surface layer of an Al alloy by friction stir processing, Journal of surface engineered materials and advanced technology, (2011), 1, 95-100.

[18] K.H. Song, W.Y. Kim, K. Nakata, Investigation of microstructure and mechanical properties on surface-modified inconel 718 alloy, materials transactions, 54, 2032-2036 (2013).

[19] K.G. Budinski, Tribological properties of titanium alloys, Wear, 151 (1991) 203-217.

[20] Y.Berthier, L.Vincent, M.Godet, Fretting fatigue and fretting wear, Tribol.Int., 22 (1989) 235–242.

[21] R.B. Waterhouse, Fretting wear in ASM handbook, Vol. 18. (ASM International, Materials Park, Ohio, 1992) pp 242-256.

[22] G.W. Stachowiak, A.W. Batchelor, Engineering tribology (Elsevier, United Kingdom, 2005) pp. 419-459.

[22] J. Qu, P.J. Blau, T.R. Watkins, O.B. Cavin, N.S. Kulkarnia. Friction and wear of titanium alloys sliding against metal, polymer, and ceramic counterfaces, Wear 258 (2005) 1348–1356.